14th International Symposium on Particle Image Velocimetry – ISPIV 2021
August 1–5, 2021

Volumetric Lagrangian Particle Tracking of the water surface flow produced during the movement of a mechanical insect leg

Thomas Steinmann[1*], Laurent David[2], Patrick Braud[2], Jérôme Casas[1]

[1] Institut de Recherche en Biologie de l'Insecte, IRBI UMR CNRS 7261, Tours, FRANCE

[2] Institut PPrime, UPR 3346, CNRS-Université de Poitiers-ENSMA, France

[*] thomas.steinmann@univ-tours.fr

Abstract

Over a thousand animal species are capable of walking on the interface between air and water. These species include water striders, a family of insects from the order Hemiptera that has an almost unique ability to walk on the surface of the water without penetrating it. They achieve this outstanding feat by making use of the surface tension and their long hydrophobic legs. Experiments have revealed that water striders transfer some momentum to the underlying fluid through capillary waves and hemi-spherical vortices and that both waves and vortices contribute to the mechanism of propulsion. However, the exact momentum and energy carried by waves and vortices have never been quantified together, and only the energy of the surface waves has been quantified to date. An analysis of the complete energy balance between the interface and the body of the water requires measurement of the free surface topography, together with the three-dimensional (3D) flow field in the water under the surface. The ultimate aim of this work was to develop a method capable of doing this.

1 Introduction

Water striders (1.a) are semi-aquatic bugs that slide on the surface of ponds, using their hydrophobic legs to move. We seek to understand the physical mechanisms of momentum exchanged, involved during the propulsion of these insects. These mechanisms are twofold, (i) on one hand the insect legs exchange momentum with the air/water interface through the emission of capillary-gravitational waves ((Steinmann et al. (2018))) and (ii) on the other hand the insect transfers momentum under the water surface (1.b). This exchange, under the water surface, is realized through pressure and viscosity forces and results in the emission of a semi-annular vortex (1.b, (Steinmann et al. (2021b)). A leg pushes a much larger volume of water than itself and thus acts as a virtual oar made of leg-plus-dimple (1.a). The uniqueness of the water strider locomotion is due to the presence of this added mass of water, absent in most other organisms moving at the air-water interface. Our ultimate goal is to achieve a complete energy balance evaluation of this interfacial flow. It requires simultaneous coupled estimations of the free surface topography and of the flow velocity beneath the surface. The combined estimation of the interface topography and the 3-D velocity field below the interface is especially challenging. The choices we made, concerning laser illumination direction, camera position and water tank geometry, have consequences. For instance, the side illumination of a wavy air–water interface often results in the appearance of shadow patches at the surface, due to wave crests. These shadow patches sometimes prevented the identification of the particles at the interface. We proposed and developed an advanced method which circumvents some of these limitations. This technique will be tested on an artificial mechanical insect leg, mimmicking the movement of a water strider leg during propulsion.

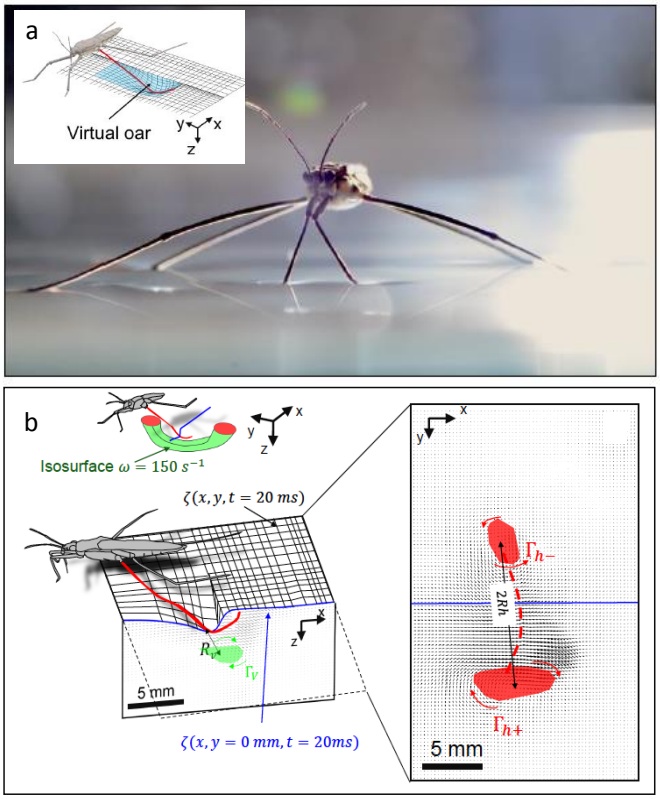

Figure 1: Water strider, virtual oar and vortices produced bellow the air-water interface during the propulsion. (a) Photograph of Gerris palludum and illustration of the virtual oar geometry during propulsion in perspective view. The virtual oar is the leg-plus-dimple that pushes a much larger volume of water than the leg itself. (b) Dynamics of surface topography and bulk flow during the propulsion of a water strider. Three-dimensional snapshot representation of body position, surface topography and vorticity isosurface in the underlying fluid. We also illustrate the flow velocity field in the fluid at the interface. The estimated position of the leg is indicated as a dotted red line. The two counter-rotating cylinders typical of a dipolar vortex are visible (Figures from Steinmann et al. (2021b)).

2 Volumetric Lagrangian Particle Tracking

We applied an extension of the volumetric LPT technique to this coupled measurement (2.a, Steinmann et al. (2021a)). Our original setup made it possible to monitor, in real time, the 3D position of fluorescent tracer particles, both on the surface and in the bulk flow. We overcame the shadow effect due to the presence of waves at the interface by illuminating the flow through the underside of a truncated squared pyramidal water tank. We chose to use a water tank of this shape to ensure that optical access could be established orthogonally through the walls of the tank. Four high-speed cameras were focused on the illuminated volume of the flow through the four lateral sides of the pyramidal water tank. The images of the four cameras were analyzed by 3D Lagrangian particle tracking velocimetry. With this technique, we were able to track particles accurately at seeding densities compatible with the thresholds for tomographic PIV and to reduce considerably the number of ghost particles. We then obtained local 3D velocities by interpolating vector volumes from the discrete particles.

3 Artificial mechanical insect leg measurements

However, it is difficult to accurately characterize the forces exchange involved in the water striders propulsion because of the lack of reproducibility in their legs movement (Steinmann et al. (2021b)). Therefore,

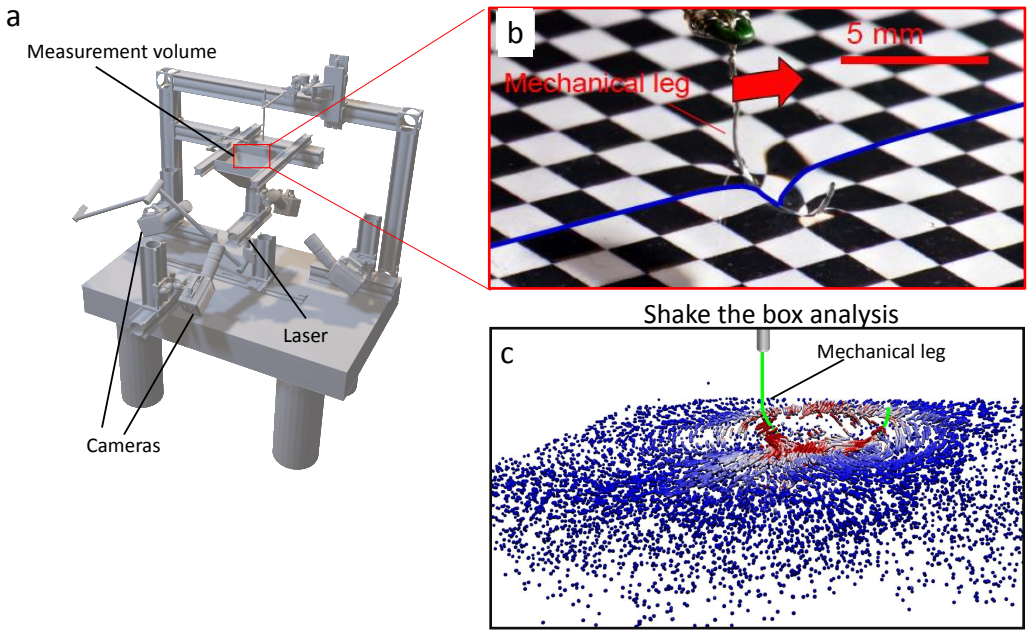

Figure 2: (a) Volumetric LPT experimental setup for the visualization of moving artificial leg at air-water interface. The mechanical leg is guided by a translation plate. The previously seeded flow and the air / water interface are illuminated by a laser volume. (b) Photography of the mechanical leg pushing down the air-water interface statically. A micromanipulator, placed on the translation plate, allows us to precisely position the leg on the interface. The static leg initially exerts pressure on the interface creating a meniscus. The blue line figures out the vertical cross section of the initial deflection of the air-water interface. (c) Result of the shake the box analysis of the flow produced during the movement of the artificial leg.

we designed a mechanical system that mimics the kinematics of the insect legs (2.b). We simulated the water strider leg using a cylinder (D = 0.1 mm, L = 40 mm) made of steel, of identical diameter and similar length to real animals. It has been shown that the leg may undergo a large deformation while pushing on the air–water interface. The curved shape of the mechanical leg was chosen to mimic the deformed shape of the tarsi. This shape, which is similar to the curvature of interface, greatly reduces the forces exerted on the air–water interface and prevents its breaking while sculling at high velocity. The surface was furthermore covered with a super-hydrophobic coating (Ultra ever Dry, TAP France, Plaisir), which reproduced the hydrophobic characteristic of natural legs and allowed us to reach a contact angle of 175 degrees, very close to the 168 degrees of *Gerris* legs. The mechanical leg was held by a micromanipulator (Newport M-MT-AB2) placed on a horizontal translation stage (Throlabs DDSM50) and positioned in contact with the water surface. The translation stage allowed a precise movement along the x axis at a velocity of 25 cm/s. Using this mechanical device, we were able to reproduce accurately the water strider legs kinematic. The use of the artificial leg allows us to generate both capillary-gravitational waves and half-ring vortex, as involved in the insect locomotion (2.c). The energy balance was determined by evaluating interface position and bulk flow velocity. Surface curvature and potential energy were determined from surface topography. The kinetic energy of the flow was derived from the bulk flow velocities.

4 Results and Conclusions

Our 3D PTV measurements allow us to determine the dynamics of the air–water interface topography and bulk flow velocity, as presented in 3. The artificial leg pushes down and creates a depression of the free surface. The interface is rapidly displaced by the leg. This displacement of the water surface establishes the boundary conditions between air and the underneath fluid. There is an immediate generation of vorticity, as seen by the two vortices in the (x, y) plane (3). The vortex also develops under the interface in the (x, z) plane. According to Helmholtz's theorem, a vortex line cannot start or end in the fluid, but must end either at a solid boundary or form a closed loop. In our particular case, it ends at the boundary of the fluid. Thus

these apparent three vortices form in fact a single semi annular vortex. The vortex geometry is related to the dimple geometry and closely follows the displacement of the dimple. The vorticities, circulations and velocities are large in both horizontal and vertical plane, the vortex being flattened in the horizontal plane.

To validate the accuracy of the 3D reconstruction of the flow, we compared these 3D measurements (4.a) to 2-D PIV measurements on the same mechanical leg moving at the same depth and same velocity (4.b), as already presented in Steinmann et al. (2021b). This comparison of mechanical experiments shows that the 3D PTV results are quite robust, even for key details, such as the temporal changes in dimple morphology, or the magnitudes of the bow wave. When starting a stroke, the meniscus is symmetrical. As velocity increases, the process of momentum transfer appears. In 4, we notice the growing asymmetry of the meniscus, reflecting an increase of the water surface resistance. The posterior and anterior angles of the dimple deformation are similar in both experiments. The progressive increase of the bow wave and its shape are also similar.

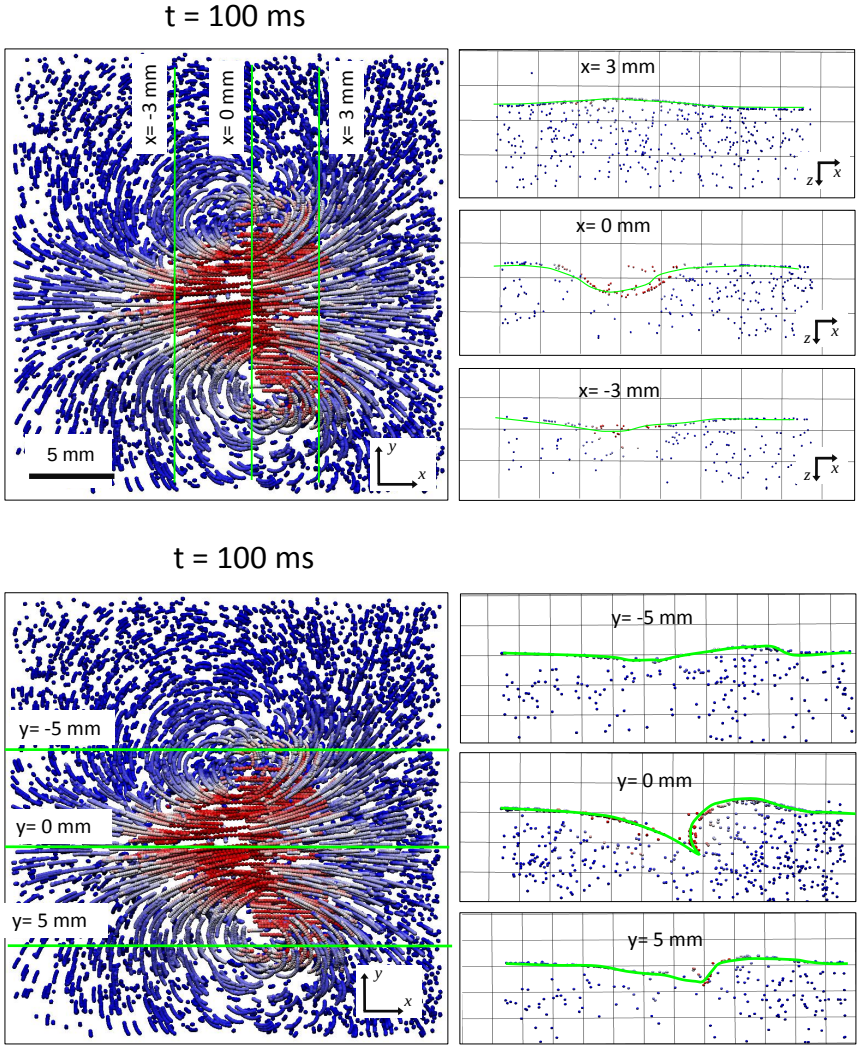

Figure 3: Snapshot of the superimposed tracked particles at the surface and in bulk flow at t = 100 ms (Δt=10 ms) during the during the movement of a mechanical insect leg curving the interface. The green lines represents the x-axis (x= -3, 0 and +3 mm) and y-axis (y= -5, 0 and +5 mm) vertical cross-section, depicted in the right panels. In these 6 panels, the green lines represent the cross sections of the interface.

We have numerically computed the interfacial flow during the sculling of a leg using finite-element simulations (5.c). We modelled the air–water interface as a diffuse interface using the phase field method implemented in Comsol Multiphysics 5.3 (COMSOL, Inc®) (Steinmann et al. (2021b)). These simulations

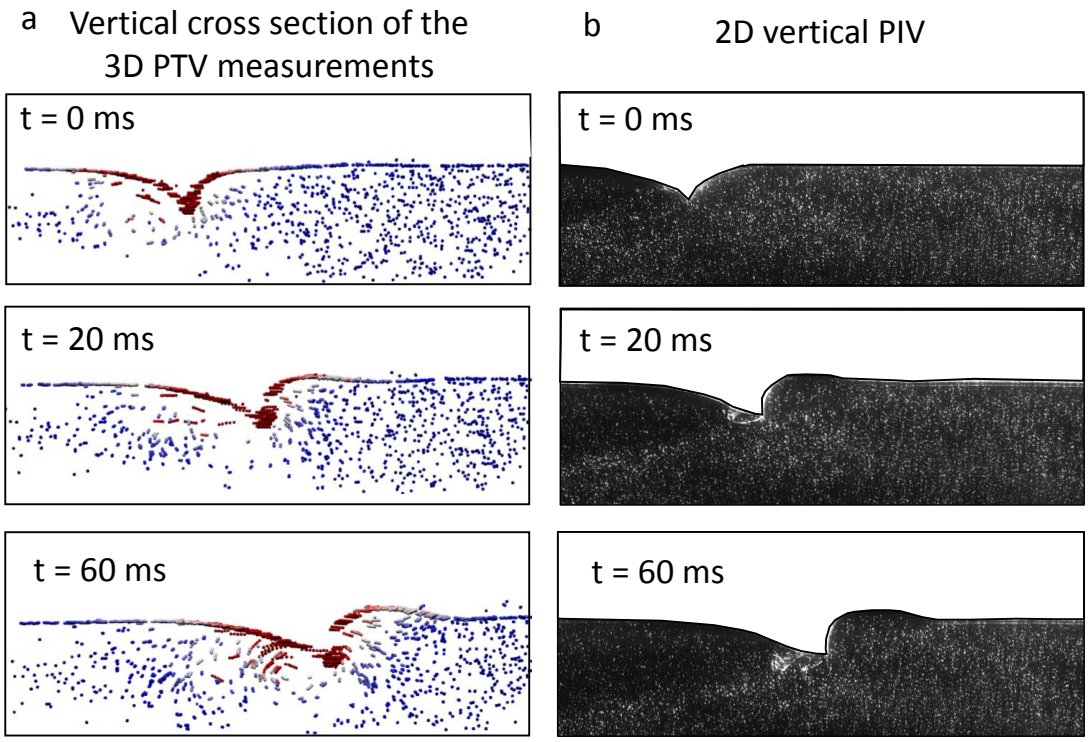

Figure 4: Comparison between a cross section of the 3D PTV experiments and 2D vertical PIV experiments of the dynamics of the interface and underlying flow during the transverse motion of a model leg. The depth of propulsion was h_l = 3 mm and the velocity was V_l = 25 cm/s. (a) Snapshots at 3 differents times (t=0ms, t=20ms, t=60 ms) of the cross section of the reconstructed position of particles from 3D PTv measurements. (b) Snapshot of the vertical cross-section of the seeded water flow and of the surface, as obtained by the high-speed camera. The complete 2D vertical PIV setup is described in details in Steinmann et al. (2021b)

have been validated with the results of the 2-D PIV experiments with a mechanical leg, to quantify the pressure forces in the fluid. We show that the pressure drag force acts on the dimple, as illustrated on 5.c. In this example, the presence of a zone of large pressure (Δp = 30 Pa) in the 3 mm high bow wave indicates that the pressure force acts essentially on this bow wave.

We prove that water strider locomotion at the air-water interface is, thus, very effective and different from flying and swimming. In flying animals, drag and lift, the forces resisting wing movement during flight, are integrated over the entire surface of the wing. The wing serves as both the physical interface on which the forces are integrated and the interface pushing the fluid. In striders, the forces act on the large meniscus that pushes the fluid, like an oar blade, rather than the tiny leg. The size of this virtual oar is function of both hydrophobicity-enhancing structural and material properties and leg kinematics.

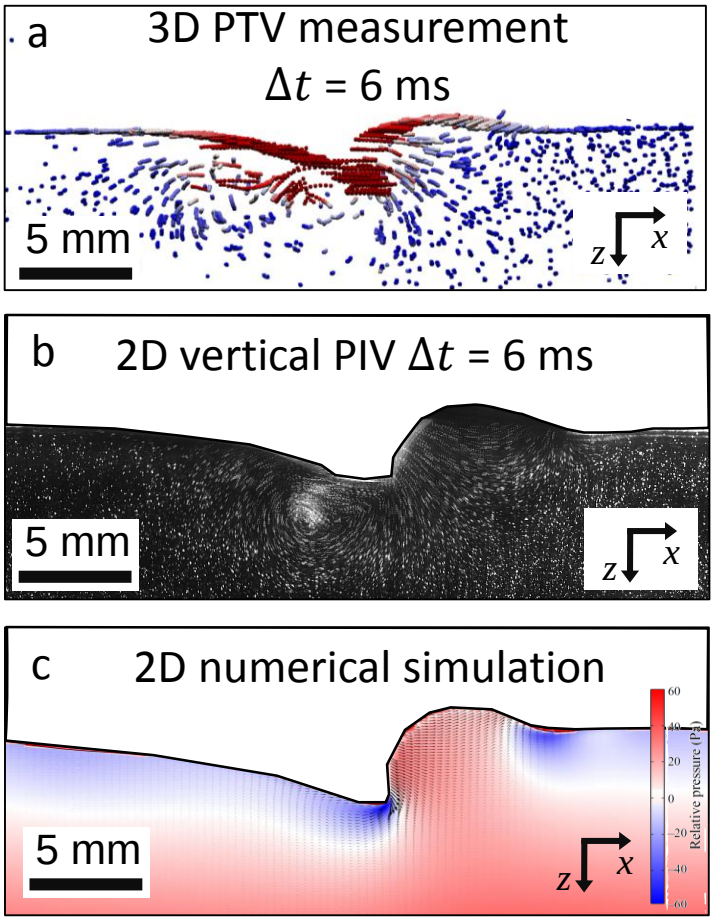

Figure 5: Comparison between 3D PTV experiments (a) and 2D vertical PIV experiments (b) and numerical simulations (c) of the dynamics of the interface and underlying flow during the transverse motion of a model leg. Numerical simulation of the pressure force acting on the moving dimple resulting from the displacement of a leg at a depth of h_l = 3 mm and a velocity of V_l = 25 cm/s. This figure illustrates the equivalence between the magnitude of the capillary force Fs acting on the leg and the magnitude of the drag pressure force F_{dimple} acting on the dimple. The presence of a zone of high pressure (Δ_p = 30 Pa) in the 3 mm high bow wave indicates that the pressure force acts essentially on this part of the virtual oar, where the bow wave appears. The resulting pressure drag force (per unit length) can be obtained by multiplying this pressure by the height of the wave to obtain F_{dimple} = 0.90 N/m.

References

Steinmann T, Arutkin M, Cochard P, Raphaël E, Casas J, and Benzaquen M (2018) Unsteady wave pattern generation by water striders. *Journal of Fluid Mechanics* 848:370–387

Steinmann T, Casas J, Braud P, and David L (2021a) Coupled measurements of interface topography and three-dimensional velocity field of a free surface flow. *Experiments in Fluids* 62:1–16

Steinmann T, Cribellier A, and Casas J (2021b) Singularity of the water strider propulsion mechanisms. *Journal of Fluid Mechanics* 915:1–31